This article was downloaded by: *[University of California, Berkeley]*
On: *24 January 2011*
Access details: *Access Details: [subscription number 929586208]*
Publisher *Taylor & Francis*
Informa Ltd Registered in England and Wales Registered Number: 1072954 Registered office: Mortimer House, 37-41 Mortimer Street, London W1T 3JH, UK

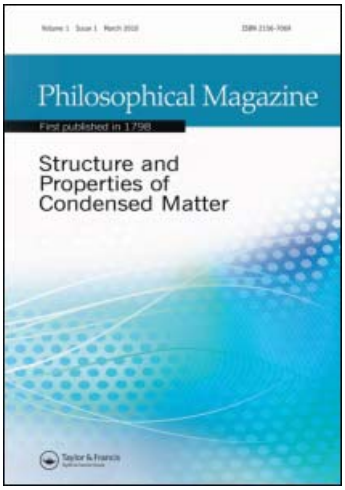

Philosophical Magazine
Publication details, including instructions for authors and subscription information:
http://www.informaworld.com/smpp/title~content=t713695589

Supercritical fluid behavior at nanoscale interfaces: Implications for CO_2 sequestration in geologic formations

D. R. Cole[a]; A. A. Chialvo[a]; G. Rother[a]; L. Vlcek[bc]; P. T. Cummings[b]
[a] Chemical Sciences Division, Oak Ridge National Laboratory, Oak Ridge, TN 37831-6110, USA [b] Department of Chemical Engineering, Vanderbilt University, Nashville, TN 37235, USA [c] Institute of Chemical Process Fundamentals, Academy of Sciences of the Czech Republic, 165 02 Prague 6, Czech Republic

First published on: 31 March 2010

To cite this Article Cole, D. R. , Chialvo, A. A. , Rother, G. , Vlcek, L. and Cummings, P. T.(2010) 'Supercritical fluid behavior at nanoscale interfaces: Implications for CO_2 sequestration in geologic formations', Philosophical Magazine, 90: 17, 2339 — 2363, First published on: 31 March 2010 (iFirst)
To link to this Article: DOI: 10.1080/14786430903559458
URL: http://dx.doi.org/10.1080/14786430903559458

PLEASE SCROLL DOWN FOR ARTICLE

Full terms and conditions of use: http://www.informaworld.com/terms-and-conditions-of-access.pdf

This article may be used for research, teaching and private study purposes. Any substantial or systematic reproduction, re-distribution, re-selling, loan or sub-licensing, systematic supply or distribution in any form to anyone is expressly forbidden.

The publisher does not give any warranty express or implied or make any representation that the contents will be complete or accurate or up to date. The accuracy of any instructions, formulae and drug doses should be independently verified with primary sources. The publisher shall not be liable for any loss, actions, claims, proceedings, demand or costs or damages whatsoever or howsoever caused arising directly or indirectly in connection with or arising out of the use of this material.

Philosophical Magazine
Vol. 90, Nos. 17–18, 14–28 June 2010, 2339–2363

Taylor & Francis
Taylor & Francis Group

Supercritical fluid behavior at nanoscale interfaces: Implications for CO_2 sequestration in geologic formations

D.R. Cole[a]*, A.A. Chialvo[a], G. Rother[a], L. Vlcek[bc] and P.T. Cummings[b]

[a]*Chemical Sciences Division, Oak Ridge National Laboratory, Oak Ridge, TN 37831-6110, USA;* [b]*Department of Chemical Engineering, Vanderbilt University, Nashville, TN 37235, USA;* [c]*Institute of Chemical Process Fundamentals, Academy of Sciences of the Czech Republic, 165 02 Prague 6, Czech Republic*

(*Received 7 August 2009; final version received 23 November 2009*)

Downloaded By: [University of California, Berkeley] At: 19:51 24 January 2011

Injection of CO_2 into subsurface geologic formations has been identified as a key strategy for mitigating the impact of anthropogenic emissions of CO_2. A key aspect of this process is the prevention of leakage from the host formation by an effective cap or seal rock which has low porosity and permeability characteristics. Shales comprise the majority of cap rocks encountered in subsurface injection sites with pore sizes typically less than 100 nm and whose surface chemistries are dominated by quartz (SiO_2) and clays. We report the behavior of pure CO_2 interacting with simple substrates, i.e. SiO_2 and muscovite, that act as proxies for more complex mineralogical systems. Modeling of small-angle neutron scattering (SANS) data taken from CO_2–silica aerogel (95% porosity; ~7 nm pores) interactions indicates the presence of fluid depletion for conditions above the critical density. A theoretical framework, i.e. integral equation approximation (IEA), is presented that describes the fundamental behavior of near-critical adsorption onto a non-confining substrate that is consistent with SANS experimental results. Structural and dynamic behavior for supercritical CO_2 interaction with muscovite ($KAl_2Si_3AlO_{10}(OH)_2$) was assessed by classical molecular dynamics (CMD). These results indicate the development of distinct layers of CO_2 within slit pores, reduced mobility by one to two orders of magnitude compared to bulk CO_2 depending on pore size and formation of bonds between CO_2 oxygens and H from muscovite hydroxyls. Analysis of simple, well-characterized fluid-substrate systems can provide details on the thermodynamic, structural and dynamic properties of CO_2 at conditions relevant to sequestration.

Keywords: geologic sequestration; nanostructures; supercritical CO_2; adsorption; integral equation calculation; molecular dynamics

1. Introduction

Over the past 10 years, carbon dioxide capture and sequestration (CCS) in deep geological formations has emerged as an important component of the portfolio of options for reducing greenhouse gas emissions. To have a significant impact on the reduction of global greenhouse gas emissions, huge volumes of CO_2 must

*Corresponding author. Email: coledr@ornl.gov

ISSN 1478–6435 print/ISSN 1478–6443 online
© This work is published by permission of the US Department of Energy under Contract No. DE-AC05-00OR22725. The US Government retains for itself, and others acting on its behalf, a paid-up, non-exclusive, and irrevocable worldwide licence in said article to reproduce, prepare derivative works, distribute copies to the public, and perform publicly and display publicly, by or on behalf of the government.
DOI: 10.1080/14786430903559458
http://www.informaworld.com

be sequestered. Large sedimentary basins can provide geological formations with sufficient pore space to accommodate these large volumes of supercritical CO_2 [1]. They contain vast volumes of inter-layered sedimentary rocks of different textures and compositions that provide both the pore volume to sequester the CO_2 and impermeable seals to trap the CO_2 underground. Suitable formations should be deeper than 800 m, have a thick and extensive seal (e.g. shale, fine-grained mudstone), sufficient porosity to contain large volumes of CO_2 and enough permeability to permit injection of CO_2 at high flow rates without overly large pressure buildup [2]. In most sequestration scenarios, CO_2 is injected in liquid form (low T, modest to high P), but transforms to a supercritical fluid as it enters the formation and is heated to formation temperatures typically exceeding 40°C. Within sedimentary basins, depleted oil and gas reservoirs, salt-water filled aquifers (or saline aquifers) and coal beds are all options for sequestering CO_2 [3].

Four trapping mechanisms can contribute to retention of CO_2 over long periods [4]: structural (or hydrodynamic trapping), capillary trapping (also called residual phase trapping), solubility trapping, and mineral trapping. The relative importance of these mechanisms changes over time, as CO_2 migrates and interacts with the rocks and indigenous formation fluids. Of these, structural trapping provided by the cap (seal) rock or other suitable aquitards, such as a shale, mudstone or evaporite layer, has been recognized as the primary mechanism affecting the long-termed CO_2 storage integrity [5,6]. A number of features contribute to the effectiveness of cap rock CO_2 containment including a thick, laterally extensive unit, well-developed bedding and minimal fracturing, high clay and low sand and silt content, parallel-preferred orientation of the clays and related pore-openings, and small nanoscale pore throat dimensions [7–11]. The ultimate sealing mechanisms are low porosity-low permeability combined with high capillary entry pressures [3].

Recent modeling suggests that a significant proportion of the CO_2 injected into geologic storage sites may escape by diffusion through cap rock in less than 1000 years depending on the properties of the formation [12]. However, experimental studies indicate that some percentage of the "leaking" CO_2 may be retained via adsorption onto clays or other mineral surfaces in shales [13,14]. As will be discussed below, a significant fraction of the pores in shales and mudstones is dominated by pore sizes in the nano-range (<100 nm). We know that the behavior of both simple and complex fluids in nanoconfined geometries (pores, fractures) will have a significant impact on behavior of fluids in the cap rock environment. The influence of confinement on the structure and dynamics of geo-fluids is now starting to receive more attention [15–23]. The behavior of fluids in nanopores typically differs from their bulk counterpart due to the presence of solid–fluid interfaces that induce pronounced local density inhomogeneities. A number of factors dictate how fluids and, with them, reactants and products of intrapore transformations migrate into and through these nano-environments, wet, adsorb and ultimately react with the solid surfaces. These include the size, shape, distribution and interconnectedness of these confined geometries, the chemistry of the solid (e.g. hydrophophic versus hydrophilic surfaces), the chemistry of the fluids and their physical properties ([21,23] and references therein). Within any rock environment there will be a great deal of heterogeneity exhibited by the pore features.

Downloaded By: [University of California, Berkeley] At: 19:51 24 January 2011

At present, we still lack a fundamental understanding of the structural and dynamic behavior of CO_2 (and CO_2-bearing fluids) in cap rock environments dominated by nanoporosity, particularly for state conditions encountered in injection systems. Even for a simple fluid such as CO_2 we have not adequately explored interfacial phenomena such the wetting and adsorption for variable pore sizes and pore geometries (e.g. cylindrical versus slit) and pore wall chemistry at conditions approaching and crossing into the supercritical regime. Nor have we thoroughly documented the dynamical behavior of CO_2 under confinement as a function of key pore features and state conditions. This communication addresses four interrelated topics: (i) the nature of nanoporosity in shales and mudstones, (ii) key experimental results on CO_2–matrix interactions relevant to sequestration, (iii) a theoretical assessment of the adsorption behavior of gaseous and supercritical CO_2 interacting with a SiO_2 substrate and (iv) a new description of the dynamical behavior of CO_2 in slit pores (muscovite). Emphasis is placed on interrogation of CO_2 at supercritical conditions in model-substance nanopores.

Downloaded By: [University of California, Berkeley] At: 19:51 24 January 2011

2. Nanoporosity and mineralogy in cap rocks

Porosity and permeability are the key variables that link the thermal, hydrological, geochemical and geomechanical processes that redistribute mass and energy in response to the disequilibrium state imposed by injection of CO_2 into the subsurface [24]. In the case of cap-rock formations, the sealing quality is arguably the most critical factor controlling the vertical migration of overpressurized or buoyant fluids, such as CO_2, in an injection system. The sealing properties of the cap rock depend on pore features, i.e. size, shape, distribution, etc., as well as the properties of the pore fluid, such as density and interfacial tension (IFT). The pore features are influenced by depositional setting and original mineralogy [25], sediment compaction [26,27], burial depth and diagenetic alteration [7,28,29], and deformation history [30]. In general, there is a linear relationship between increasing porosity and increasing permeability; for shales and clay-rich mudstone porosities range from a few percent to as much as 20 for permeabilities (transport normal to bedding) ranging from 10^{-22} to $10^{-19}\,m^2$ [8,11]. A linear relationship has also been observed between porosity and mean pore throat size for select clay-bearing mudstones; for porosities between 5–10%, mean pore throat sizes range from <5 to 10 nm [11]. Pore throat sizes approaching 100 nm correlate with porosities >10% up to 20%. Pores can exhibit a number of geometries including slits as cleavage-parallel voids, bedding-parallel cracks or terminations of stacked clay platelets (definitions from [10]) (Figure 1a), cylinders formed at grain triple junctions, along grain boundaries (Figure 1b) or within a reaction layer (Figure 1c), and irregular voids exhibiting both cylindrical and slit-like characteristics commonly observed at clay–detrital grain contacts, as minute fractures in detrital grains or as dissolution features (Figure 1d).

As one might expect for cap rocks, there is a relationship between porosity, permeability and mineralogy, although the role of mineralogy and mineral texture is still poorly constrained. There is a general tendency for the more clay-rich rocks to exhibit lower porosities and permeabilities [8,10,31]. This is in part due to the fact

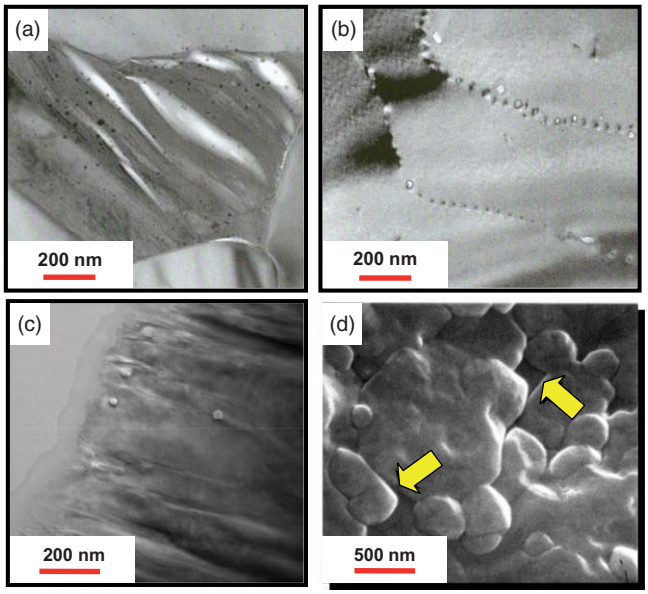

Figure 1. Transmission electron micrographs of representative pore features in natural materials. (a) Slit pores in kaolinite. (b) Cylindrical pores formed along a grain boundary. (c) Cylindrical pores formed in a albite replacement front. (d) Dissolution-derived capillary-shaped pores in fine grained quartz.

that a number of factors contribute to porosity in addition to mineralogy, such as fraction and size of non-clay detrital grains (e.g. quartz, feldspars, lithic fragments), grain orientation, organic content and depth of the formation. Mineral abundances for representative shales are presented in Table 1. The total clay content for these examples ranges from ~50 to over 70% with illite–smectite, chlorite or mica dominating. Thus, it is understandable why a significant fraction of the porosity in shales falls within the nanoscale range, <100 nm. The remaining mineral fraction is typically dominated by fine-grained quartz so, in simple terms, a shale may be considered a quartz-clay rock. With this in mind, results presented below describe our effort to interrogate the behavior of CO_2 interactions with both a pure SiO_2 substrate (as a proxy for quartz) and a muscovite substrate (a proxy for the mica fraction) over nanopore length scales that fall within the lower and upper range observed for shales and shaley mudstones, i.e. ~1 to 100 nm.

3. Experimental behavior of CO_2 in nanopores

A wide variety of experimental methods have been used to assess the behavior of both sub- and supercritical CO_2 in nanoporous environments including but not limited to volumetric and gravimetric adsorption, nuclear magnetic resonance spectroscopy (NMR), infrared spectroscopy (IR) and neutron scattering (NS). A limited body of work has been presented for CO_2 interaction with bulk rock or minerals such as shale [32,33], clays [13,14] and granite [34]. Coals from different geologic sites were studied to assess the influence of moisture on storage capacity and

Downloaded By: [University of California, Berkeley] At: 19:51 24 January 2011

Downloaded By: [University of California, Berkeley] At: 19:51 24 January 2011

Table 1. Average mineral contents (wt. %) from representative shales, a number of which act as caprocks.*

	USA				NORWAY		CANADA			AUSTRALIA	UNITED KINGDOM		ITALY (i)		
Formation or site:	Frio (a)		Wilcox (b)	New Albany (c)	Sleipner (d)	Draupne (e)	Venture gas field (f)			Muderong (g)	Kimmeridge (h)		AVC	IFR	EFR
Phase	2133′	4572′			Lower seal		LSC	LSD	INT		KWC	KBC			
Quartz	20.7	22.6	35	43	30	35.7	61	45	43	27	25	30	16.2	28.1	19.7
K-feldspar	3.1	0.7	5	5.1	5	2.5	3	3	4	2			5.2	3.9	1.9
Plagioclase	3.9			1.4		1.6									
Albite		5.2			2					1					
Illite–smectite	41.3	49.3	2	16	3 (sm)	14.6 (sm)	3	6.5	9	28 (sm)	20	10	39	47.9	49.7
Illite	12.4	8.8	29	16		9.2							5	6.8	8.8
Mica					30		10	24	33	17	25	20			
Kaolinite	16.8	9.7	10		14	12.3	3	9		15			4.8	1.0	16.3
Chlorite	1.8	3.7	14	6	1	3.4	4	4	10	5	10	30	23.3	4.2	2
Chlorite–smectite												Trace		5.3	
Calcite			2	2.4	3		8	4			15	>5	5.3	0.2	
Dolomite						14.6	2	1					1.2		
Ankerite															
Hematite													0.1	2.8	1.6
Pyrite				6.5	1	6.1	4	3.5		2	5	>5			
Barite					5										
Organics			1.0	9.4	0.68–1.28										

Notes: (a) [103]; (b) [104]; (c) [105]; (d) [106]; (e) [107]; (f) LSC = late stage cementation, LSD = late stage dissolution, INT = intermediate characteristics [7]; (g) [108]; (h) KWC = Kimmeridge Westbury Clay, KBC = Kimmeridge Bay Clay [109]; (i) AVC = Argille Varicolori, IFR = Internal Flysch Rosso, EFR = External Flysch Rosso sediments [110].
* not all minor phases represented so totals may not = 100%.
(sm) refers to cases where smectite is the dominant phase.

sorption mechanism [35,36]. Small angle and ultra small angle neutron scattering (SANS and USANS) were used in the study of CO_2 sorption in several coals under storage site conditions in order to measure the pore fluid density as a function of pore size [37]. Methane production from coal beds, which can be enhanced by the simultaneous adsorption of CO_2 and release of natural gas, gains importance as an alternative energy source. The preferential sorption properties from CH_4/CO_2 mixtures in coal have been recently studied in [38,39], and the results indicate that the simultaneous production of methane and sequestration of CO_2 is possible, and may be an option for the use of unmineable coal beds. However, most of the work has been directed at CO_2 interactions with engineered materials, such as mesoporous silica, silica gel, zeolites and carbon. Use of engineered materials with well-characterized pore features and simplified, tunable pore wall chemistry facilitate a more complete interpretation of experimental results and their link to molecular-level modeling. Thus, CO_2 interaction with engineered silica materials may be viewed as a reasonable proxy for silica-rich nanoscale systems found in nature.

Supercritical excess adsorption isotherm (experimental) data of different gases over a wide variety of substrates typically show similar behavior. At low fluid densities, the excess sorption increases with increasing fluid pressure and density. In this region, the slope of the isotherm is controlled by the strength of the fluid–solid interactions and the degree of microporosity [40]. With increasing fluid density, the excess adsorption commonly attains more or less a pronounced maximum. This maximum occurs only for supercritical fluids. One explanation for this maximum follows from the definition of excess sorption, which is given as the integral over the difference between local (inhomogeneous) fluid density $\rho(r)$ normal to the solid surface and the bulk fluid density ρ_b: $n_e = \int_0^\infty [\rho(r) - \rho_b]\mathrm{d}r$. For simplicity, it is assumed that the sorption phase profile $\rho(r)$ remains constant with the bulk fluid density. For small ρ_b, the difference $\rho(r)$–ρ_b increases with increasing ρ_b, leading to a positive slope of the excess sorption isotherm. For larger values of ρ_b, this difference gets smaller, leading to a smaller value of the excess sorption and negative slope of the isotherm [41].

The formation of a maximum in the excess sorption isotherms of supercritical fluids has been reported for nitrogen and methane in microporous carbon and mesoporous silica [42,43], CO_2 on superactivated carbon [44], silica gel and 13X zeolite [45–47], synthetic F400 adsorbent [48] and also for shales [14]. Recent modeling based on statistical mechanics has reproduced these general features of supercritical sorption isotherms [49]. Monte Carlo simulation was used to model the excess sorption of supercritical CO_2 in zeolites [50]. Negative excess sorption data for low-density supercritical CO_2 in zeolites have been reported in [51], who invoked a sorption mechanism involving steric blocking of sorption sites and partial pore blocking effects.

In the close vicinity of, and upon approaching the critical point, the excess sorption isotherms may show a strong increase or decrease in the amount adsorbed – phenomena called critical adsorption and critical depletion. Critical adsorption effects, i.e. a sudden increase in the excess sorption at near-critical conditions, are reported for CO_2 on activated carbon [52,53] and for methane on mesoporous silica gel [43]. Critical depletion effects, expressed as pronounced decrease of the excess

Downloaded By: [University of California, Berkeley] At: 19:51 24 January 2011

sorption under near-critical conditions, have been described for SF_6 on carbon black [54] and silica [55,56].

These observations highlight the fact that the supercritical-isothermal excess adsorption on solid substrates depends on the interplay between the (density dependent) fluid–fluid interactions and the fluid–substrate interactions, i.e. on the extent of the asymmetry between the strength of the two types of interactions.

Supercritical CO_2 sorption in porous silica has been intensively studied for its importance in supercritical fluid chromatography [57]. Classical gravimetric or volumetric sorption experiments measure only the excess or Gibbs sorption, i.e. the difference between the amount of fluid in the sorption phase and the bulk fluid concentration. However, absolute adsorption, the quantity of greatest interest from a sequestration point of view, cannot be directly measured in gravimetric or volumetric sorption experiments, although models have been developed to extract absolute adsorption from excess sorption data for supercritical CO_2 in silica [44]. Since all sorption quantities are macroscopic in nature they do not provide direct information about the morphology of the sorption phase and its change with pressure and temperature. To apply sorption theory, knowledge of the density of the sorption phase and its volume (thickness) are crucial. Neutron scattering is particularly suitable for the study of sorption processes owing to its sensitivity to structures on a nm length scale, and the weak interactions of neutrons with matter allow the study of relatively thick samples (up to several mm). SANS is particularly well-suited for the study of mesoporous materials with pore sizes of 2–50 nm, and a variety of fluids imbibed in these mesopores. In some cases, contrast variation can be used as a powerful tool to simplify the scattering signal from a complex system. It is well known that liquid nitrogen matches the scattering length density of SiO_2, i.e. silica pores filled with liquid nitrogen are not visible in a SANS experiment. This effect has been used to study pore condensation phenomena and pore network hierarchy of mesoporous silica [58].

Only a few neutron scattering studies of the sorption of supercritical fluids imbibed in porous matrices exist. SANS data obtained for supercritical CO_2 confined in silica aerogel (95% porosity and 65–70 Å mesh size) by Melnichenko et al. [59] were analyzed along with new data on d-propane confined in silica aerogel with the newly developed Adsorbed Phase Model described in detail [60]. The Adsorbed Phase Model (APM) combines the Three-Phase model by Wu [61] with a mass balance consideration of the pore fluid; it yields both the mean density ρ_3 and the volume ϕ_3 of the sorption phase. It is the first experimental characterization of the sorption of pore fluids. Neutron transmission and the Lambert–Beer law have been used in [60] for the estimation of the mean density of the pore fluid, but excess sorption data measured by gravimetric or volumetric methods could also be used. Because the APM yields both mean density and volume fraction of the sorption phase, it can also be used to estimate the hitherto experimentally inaccessible quantity of absolute adsorption without further model assumptions using the formula: $n_a = \rho_3 \bullet \phi_3 \bullet V_p$.

In Figure 2a, the properties of the sorption phase (i.e. mean density and volume) are shown, whereas Figure 2b presents the sorption quantities – excess, total and absolute adsorption – given in unit mass unit of adsorbed fluid per unit mass of solid, i.e. [g/g]. Total adsorption is defined as the total amount of fluid confined in the

Downloaded By: [University of California, Berkeley] At: 19:51 24 January 2011

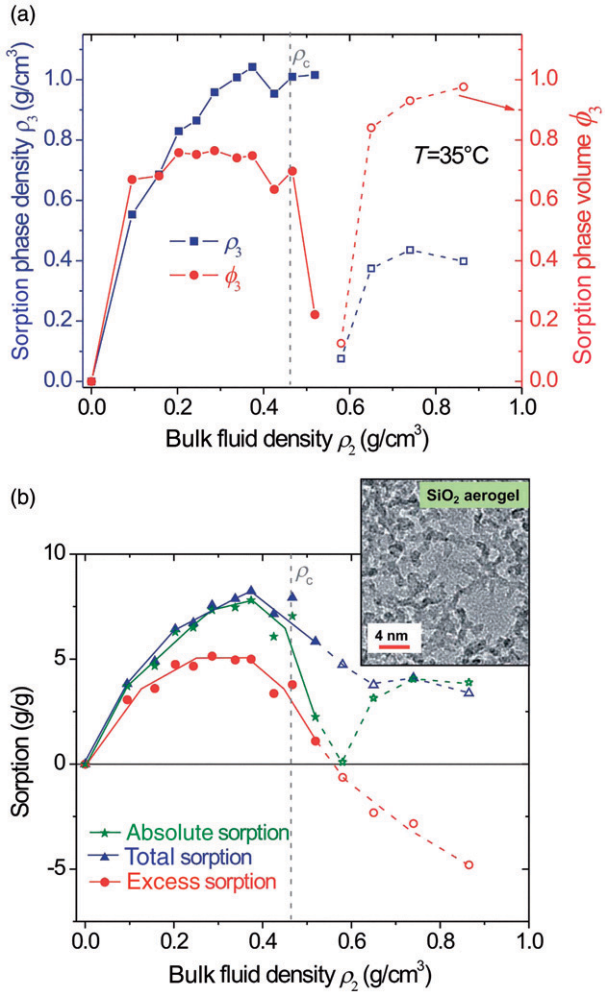

Figure 2. (Color online). Sorption isotherm of supercritical CO_2 in silica aerogel with 95% porosity, measured by a combination of SANS and neutron transmission and analyzed with the Adsorbed Phase Model ($T = 35°C$). (a) Density and volume of the sorption phase [60]. (b) Sorption quantities as calculated from the sorption phase density and volume. The dashed gray lines demarcate the value of the critical bulk density of CO_2. The inset shows a TEM image of the silica aerogel; pore walls-darker gray, pores-medium gray.

pore spaces, i.e. it is the sum of the adsorbed and unadsorbed fluid amounts. It is a measure of the uptake capacity of the solid for a given fluid at P, T. Other acceptable and often used scales, like mol/m^2 require exact knowledge of the internal surface area of the substrate. Furthermore, in the case of multilayer adsorption, the pore volume may be equally as important as the substrate surface area. Note that the calculated values of the absolute adsorption do not rely on the assumption of a constant density of the sorption phase as it is commonly the case when absolute sorption data are estimated from experimental excess sorption data.

Downloaded By: [University of California, Berkeley] At: 19:51 24 January 2011

Instead, the respective values for volume and mean density of the sorption phase were independently calculated for each point using the APM and varied non-monotonously between 0–1.07 g/cm^3 over the range of bulk fluid densities (0–0.8 g/cm^3) studied.

Initially, both the density and the volume of the sorption phase increase with increasing bulk fluid density, ρ_2. In this region, both excess sorption and absolute adsorption show a relatively steep, positive slope. This steep, positive slope culminates in a pronounced maximum in the excess and absolute sorption isotherms, centered at a bulk fluid density of $\rho_2 \approx 0.35$ g/cm^3. Under these conditions, the sorption phase has reached a maximum of $\rho_3(\max) \approx 1.05$ g/cm^3 and occupies approximately 75% of the pore volume. Further increase in ρ_2 does not significantly change the properties of the sorption phase. Hence, the difference between the bulk and sorption phase densities minimizes and a rather broad maximum is formed in the excess sorption isotherm, while the absolute adsorption remains constant. Schneider et al. [62] measured the density of near-critical CO_2 in mesoporous silica by FTIR and found a maximum density of adsorbed CO_2 of 1.07 g/cm^3, which is in good agreement with our estimate. The maximum in the density of the sorption phase is constrained to a narrow range of bulk densities below the critical density. As the fluid density approaches the critical density, the sorption phase collapses, expressed by a rapid decrease of its volume and density. Consequently, excess sorption and absolute adsorption decrease rapidly, resembling the results reported for near-critical SF_6 in Controlled Pore Glass [55,56] and our results for deuterated propane confined in silica aerogel [60]. At fluid densities above the critical density, we find negative values of the excess sorption while absolute adsorption remains positive (Figure 2b). The APM analysis suggests that a depletion phase with a density below the corresponding bulk fluid density fills the entire pore space. At high densities, i.e. in the region $\rho_2 > \rho_c$, the constancy of the neutron transmission with increasing pressure suggests a continuation of the depletion effect with increasing ρ_2.

A limited number of studies report negative values of the excess adsorption at high pressure, for instance for N_2 in silica aerogel at 138 K [43] and CO_2 in Baralaba coal [37]. There is an ongoing debate about the validity of negative values of the excess adsorption at high pressures (dashed portion of the excess adsorption curve, Figure 2b). The measurement of the excess adsorption at high pressure and density is technically difficult, requiring highly accurate measurements of the pore volume in volumetric measurements and an accurate accounting of sample buoyancy in gravimetric measurements [47]. Likewise, modeling approaches have been hampered by ambiguities and inaccuracies. A new mechanism for Monte-Carlo simulation of supercritical sorption processes was recently proposed, which avoids several ambiguities by a clearer definition of the excess sorption [63]. However, many of the studies did not probe adsorption behavior at densities far beyond the bulk critical density. The neutron transmission method for the determination of the mean fluid density in the pore space indicates depletion over a wide range of densities above the critical density, but this new method should be experimentally validated through separate volumetric and/or gravimetric sorption experiments under identical conditions. In the section below, we provide a theoretical model that describes under which conditions such high-density depletion effects may occur.

Downloaded By: [University of California, Berkeley] At: 19:51 24 January 2011

4. Molecular-based analysis and interpretation of supercritical adsorption

Adsorption of model fluids onto silica has been studied by molecular-based simulations involving Grand Canonical [64–66] and Gibbs Ensemble [50] Monte Carlo as well as molecular dynamics [67,68]. In general, these studies identify precisely defined substrate surfaces, including specific crystalline planes with no defects such as β-cristobalite [69,70], as either individual planes (plates) or parallel planes/plates to describe slit-pore structures [65,71]. Other studies targeted special types of regular porous materials, the so-called silica zeolites (structure type MFI), which are isomorphs of ZSM-5 zeolite [72]. Alternatively, slit-pores made of two amorphous silica plates obtained by the melt-quench approach [73] were used to study the interactions between supercritical carbon dioxide and silica surfaces [74].

The interrogation of these disparate model systems has provided a wealth of information on the structure and dynamical behavior of fluids undergoing adsorption onto solid surfaces. However, to gain fundamental insights into the sub- and supercritical fluid adsorption, two limiting facts stand out, namely (a) there has been no systematic approach to study adsorption phenomena from simple unconfined solid–fluid interfaces to confinement between overlapping interfaces, and (b) there is no 'clear cut' correspondence between the excess quantity ($n_e(\rho_b)$) being measured experimentally and the corresponding molecular-based calculation (Equation 4 in Appendix 1).

Real systems are neither completely crystalline nor do they have uniform pore distributions or pore-wall compositions. In fact, amorphous silica can exhibit distorted tetrahedral structures and surface defects represented by 3-coordinated silicon as well as non-bridged oxygens [75] giving rise to heterogeneous distributions of adsorption sites [68,69,76].

Most simulation studies of CO_2 adsorption on silica have involved subcritical conditions and typically targeted thermodynamic rather than structural and dynamic properties [77]. Recently, a theory has been developed by Oleinikova and Brovchenko [78], which provides a model for high-density depletion. This phenomenon, which occurs in systems with weakly attractive fluid–solid interactions, is based on the interplay between the attractive fluid–solid interactions, which dominate at low fluid densities and cause adsorption, and the missing neighbor effect of interfacial fluid molecules, which dominates at high fluid densities, causing depletion.

4.1. *Excess adsorption behavior and its near-critical solvation analogy*

The focus of this section is to provide a theoretical framework to describe the fundamental behavior of near-supercritical adsorption (relevant to CO_2 sequestration) onto a substrate under a weakly attractive regime along a near-critical isotherm by analogy to the well-established solvation behavior of dilute supercritical solutions [79]. The adsorption of a pure solvent onto a solid surface can be thought of as the limiting case of an infinitely dilute solute (the substrate), in an otherwise pure solvent, in which the relative size of the solute with respect to the solvent becomes extremely large [80]. In other words, the exposed surface of a relatively large solute can be considered as 'almost flat' for practical purposes and, in principle, we should

Downloaded By: [University of California, Berkeley] At: 19:51 24 January 2011

be able to apply the available solvation formalism for infinite dilute supercritical systems toward the interpretation of the density dependence of the excess adsorption quantities from experiment [79].

It is important to recognize a few features of the actual system that are most commonly overlooked: (a) the solid substrates and the resulting solid–fluid interfaces are never flat, (b) the solid substrates usually consist of confining spaces, i.e. pores and cavities, (c) the measured excess adsorption isotherms are actually averages over the adsorption behavior of a (not well known) combination of different types of pores (i.e. pore size and distribution) and, therefore, (d) the modeling of the excess adsorption isotherms based on a simplified picture of the Gibbs dividing surface, e.g. through a box-model, must be carefully considered when used for the interpretation of experimental data.

The approach taken here draws a parallel between the behavior of the excess adsorption (supercritical) isotherm for a pure fluid onto a surface and the Kirkwood–Buff integral (i.e. over the substrate–fluid total correlation function) for an infinite dilute solute (substrate) in an otherwise pure solvent [81], i.e.

$$G_{sf}^{\infty} \equiv 4\pi \int_0^{\infty} \left[g_{sf}^{\infty}(r) - 1 \right] r^2 \, \mathrm{d}r \tag{1}$$

where $g_{sf}^{\infty}(r)$ denotes the radial distribution function for the solute(s)–solvent(f) interactions, which describe the solvent structure around the infinitely dilute solute. Here, we purposely use 's' to denote the infinitely dilute solute because later this solute will be redefined as the solid substrate for the adsorption process.

Based on this solvation analogy, simple rigorous expressions are derived (Appendix 1) that relate relevant thermophysical properties in terms of the G_{sf}^{∞}, and then, to extract theoretical implications regarding the expected density behavior of the supercritical excess adsorption isotherm [82–85]. For example, Equations (6)–(8) indicate that the isothermal excess adsorption of imperfect gases (Henry's law regime) is positive and grows quasi-linearly with the bulk density of the fluid. As the bulk density increases along a supercritical isotherm, the contributions of the first and higher density powers in Equation (5) become more relevant, as well as the significant changes in the correlation length as a measure of the solvent isothermal compressibility. To illustrate the behavior of $n_e(\rho_b)$, according to the suggested analogy, we use integral equation calculations (IEA) based on the Percus–Yevick approximation [86] to predict the microstructure of two sets of infinite dilute Lennard–Jones solutions, representing a weakly-attractive to repulsive substrate (Figure 3) and an attractive substrate (Figure 4), respectively [82,87].

The IEA calculations in conjunction with the simple analysis presented above lead to a number of important observations. On the one hand, for a system involving either weakly attractive or repulsive solvent–surface interactions, the solvent density will exhibit a local depletion near the surface, whose effect will extend as far as the distance given by the solvent's correlation length at the prevailing state conditions, i.e. scaling as the solvent's isothermal compressibility [84]. The immediate result of the two opposite trends for the local and bulk densities is a strong decrease of $n_e(\rho_b > \rho_c)_T$ toward the negative quadrant with the appearance of a maximum near the solvent's critical density, as illustrated in Figure 3. Note that a further increase in

Downloaded By: [University of California, Berkeley] At: 19:51 24 January 2011

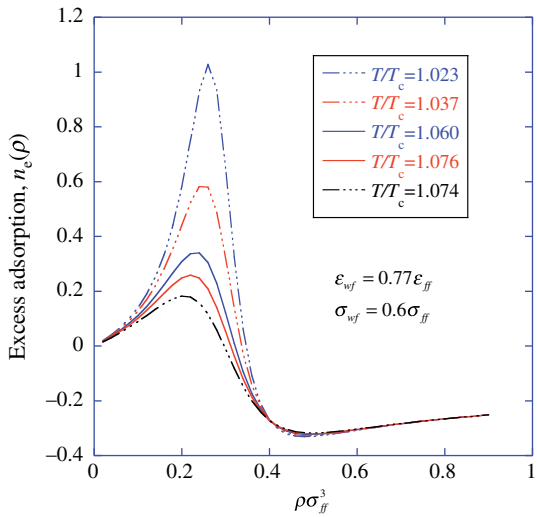

Figure 3. (Color online). Density dependence of the (dimensionless) excess adsorption from IEA calculations involving a Lennard–Jones weakly-attractive/repulsive substrate along five near-critical isotherms.

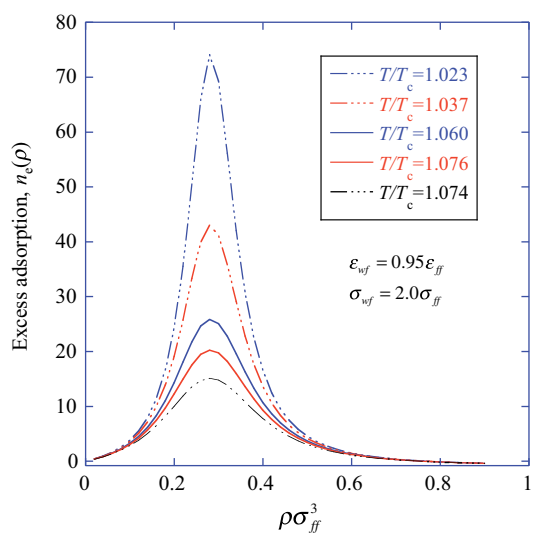

Figure 4. (Color online). Density dependence of the (dimensionless) excess adsorption from IEA calculations involving a Lennard–Jones attractive substrate along five near-critical isotherms.

bulk density reverses the above trend due to increasing solvent's packing effects and associated weakening of solvent–surface relative to the solvent–solvent interactions. The observed trends in the SANS study of supercritical CO_2 adsorption in the silica aerogel described in Section 3 are consistent with these theoretical predictions.

Downloaded By: [University of California, Berkeley] At: 19:51 24 January 2011

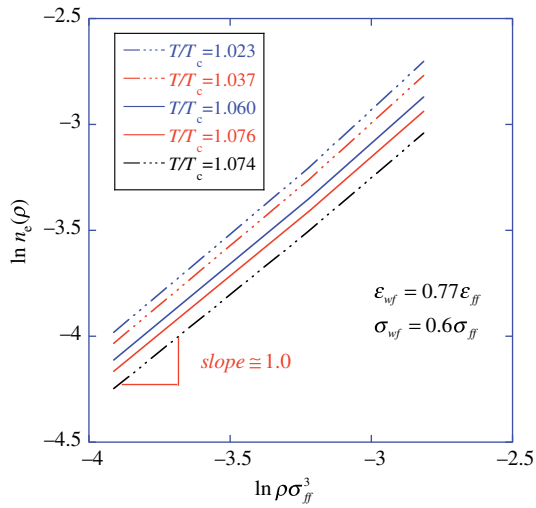

Figure 5. (Color online). $\ln n_e(\rho_b)_T - \ln \rho_b$ representation for the low-density behavior of the (dimensionless) excess adsorption from IEA calculations.

Note that the zero-density limiting slope of the $\ln n_e(\rho_b)_T - \ln \rho_b$ relationship is one (Figure 5), i.e. $n_e(\rho_b \to 0)_T \sim \rho_b$ whose constant of proportionality is $-2B_{sf}(T)$ according Equation (7). This is the manifestation of the limiting density behavior of the corresponding pair correlation function $g_{sf}(z)$ for conditions where the solvent–solvent interactions become negligibly small relative to the substrate–solvent counterpart. As the bulk density increases toward the solvent critical value along the near (but super)-critical isotherm, the solvent correlation length increases, with the simultaneous increase of the strength of $g_{sf}(z)$ and $n_e(\rho_b \to \rho_c)_T$. Further increases in the bulk density translate into different responses for the $n_e(\rho_b > \rho_c)_T$ depending on the strength of the solvent–surface relative to the solvent–solvent interactions.

On the other hand, for a system involving attractive solvent–surface interactions, the solvent density will exhibit a local enhancement near the substrate surface. Due to the attractive nature of the surface–solvent interactions, $n_e(\rho_b \to \rho_c)_T$ exhibits a profound increase in adsorption compared to that for the weakly attractive/repulsive counterpart, after the initial quasi-linear density dependence (Henry's law regime). However, as the solvent density increases beyond its critical value, the solvent's packing takes over and consequently $n_e(\rho_b > \rho_c)_T$ diminishes toward zero (Figure 4). Moreover, as expected from the temperature dependence, $B_{sf}(T)$, the low-density behavior of the excess adsorption exhibits an inversely proportional temperature dependence, i.e. $\lim_{\rho \to 0} n_e(T) \sim T^{-1}$.

Note that an interesting implication of Equations (7) and (8) involves the zero-density (pressure) extrapolation of measured isothermal excess adsorption for the estimation of the corresponding Henry's constant. If this extrapolation predicts a negative slope, then we must conclude that these anomalous low-density (pressure) isotherms are not thermodynamically consistent, and might be the result of some experimental artifact such as unattained adsorption equilibrium [51].

Downloaded By: [University of California, Berkeley] At: 19:51 24 January 2011

4.2. *CO_2 interaction with mica*

Muscovite ($KAl_2Si_3AlO_{10}(OH)_2$) and similar mica materials are known to adsorb large amounts of gasses, including carbon dioxide [88]. Desorption and X-ray photoelectron spectroscopy (XPS) experiments by Bhattacharyya [89] showed that for vacuum-cleaved mica at room temperature the surface concentration of adsorbed CO_2 molecules is approximately 44 times smaller than the concentration of potassium ions. This fact along with the second order of the adsorption reaction led to the conclusion that most adsorption sites are blocked by K^+ ions and the most likely adsorption mechanism starts by linking to hydroxyl sites and proceeds to form a bicarbonate species. Experiments with air-cleaved muscovite have shown that the surface is typically covered by a 3–4 Å thick contamination layer, which is assumed to be potassium carbonate created by the reaction of carbon dioxide with water [90,91].

Interaction of supercritical CO_2 with muscovite and similar layered silicates has received much less attention than studies with silica materials described in the previous sections. The main interest in these systems has stemmed from the industrial importance of clays as polymer fillers and supercritical CO_2 as a solvent. An example of such applications can be intercalation of CO_2 in montmorillonite with the intention to use the high diffusivity of the supercritical fluid to deliver organic molecules to otherwise inaccessible slit pores [92]. An IR spectroscopy study of CO_2 intercalation in annealed mica samples indicated that molecular species can develop from carbonates at high temperatures around 1000 K [93]. The thermodynamic aspects of sub- and supercritical CO_2 adsorption in pillar clays were investigated using the Gibbs ensemble Monte Carlo simulations [94]. The structural and dynamic properties of CO_2 confined in slit pores between talc plates at slightly supercritical 308.2 K were investigated by molecular dynamics simulations [95].

In this section, we describe the structure and diffusion of pure CO_2 in slit pores between muscovite plates at temperatures and pressures relevant for a typical sequestration reservoir. Although CO_2 intercalation in clays is anticipated to be a dominant process in shales, we use muscovite–CO_2 interaction as a proxy for an "illite/mica" system. Clearly, unlike potential CO_2 invasion into the expandable interlayers of a 2 : 1 clay such as montmorillonite, CO_2 behavior in muscovite is intended to provide insights to the structural and dynamical behavior within a very simple slit-pore model system. CO_2 molecules are represented by the EPM2 model [96] optimized to reproduce critical properties in a manner similar to related simulations studies of CO_2 in clay and silicate materials [95,97]. Muscovite is modeled by the fully flexible forcefield of Heinz at al. [98]. All atom–atom pair interactions consist of a Lennard–Jones (LJ) term and a Coulombic interaction of point charges:

$$u_{ij}(r_{ij}) = 4\varepsilon_{ij}\left[\left(\frac{\sigma_{ij}}{r_{ij}}\right)^{12} - \left(\frac{\sigma_{ij}}{r_{ij}}\right)^{6}\right] + \frac{q_i q_j}{4\pi\varepsilon_0 r_{ij}}, \tag{2}$$

where r_{ij} is the distance between sites i and j, σ_{ij} and ε_{ij} are LJ parameters for i–j interaction and q_i is the charge of site i. Partial charges and LJ parameters are listed in Table 2. The cross terms of the LJ potential were obtained from the Lorentz–Berthelot combining rules. While the same approach to cross interactions was used

Downloaded By: [University of California, Berkeley] At: 19:51 24 January 2011

Table 2. Potential parameters for CO_2 [96] and muscovite [98] used in the simulations.

Atoms	q_i [e]	σ_{ii} [Å]	ε_{ii} [kcal/mol]
C (CO_2)	0.6512	2.757	0.056
O (CO_2)	−0.3256	3.033	0.16
K	1.0	3.385	0.2
Si	1.1	3.564	0.05
Al (surface)	0.9	3.742	0.05
Al (octahedral)	1.45		
O (surface)	−0.55 (−0.78333)	3.118	0.025
O (apical)	−0.75833		
O (hydroxyl)	−0.68333		
H	0.2	0.978	0.013
Non-bonded par.		σ_{ij} [Å]	ε_{ij} [kcal/mol]
Si–C (CO_2)		2.607	0.172
Si–O (CO_2)		2.745	0.291
Al–C (CO_2)		2.6805	0.172
Al–O (CO_2)		2.8192	0.291
Harmonic bonds	r_0 [Å]	k_r [kcal/(mol · Å^2)]	$u = k_r(r - r_0)/2$
C–O	1.149	295.4	
O–H	0.929	990	
(Si, Al)–O	1.05 ∗ exp.[a]	860	
Harmonic angles	Θ_0 [deg]	k_Θ [kcal/(mol · rad^2)]	$u = k_\Theta(\Theta - \Theta_0)/2$
Al–O–H	116.2	23	
(Si, Al)–O–(Si, Al)	exp.[a]	340	

Note: [a][102].

in [95], Qin et al. [97] optimized CO_2–silica LJ parameters based on *ab initio* calculations. Most notably, the latter method produced smaller σ_{ij} parameters for Si–O interactions, which, in our case, may have consequences for the formation and stability of hydrogen bonds between CO_2 and muscovite hydroxyls.

The systems consist of two composite layers of muscovite (each ∼21 Å thick) and various amounts of carbon dioxide filling space between the two surfaces (Figure 6). The size of the simulation cell in the directions parallel to the layers is 55.4 × 53.47 Å. The size in the perpendicular direction, as well as the pore width, varies with the amount of confined carbon dioxide and pressure. LAMMPS software [99] was used to perform molecular dynamics simulations in the anisotropic NPT ensemble with temperature set to 333 K (60°C) and pressures ranging between 50 and 300 bar. The temperature and pressure were held constant using the Nosé–Hoover thermostat and barostat. Long-range Coulombic forces were computed using the 3-dimensional PPPM method with the real space cutoff distance set to 11.0 Å. The system was equilibrated for 1.0 ns and production runs covered another 1.0 ns with a time-step of 1.0 fs.

The simulations were carried out with amounts of confined CO_2 equal to integer multiples of 2.467 g/cm^2 of surface. These numbers were chosen because they roughly correspond to the amounts of CO_2 in distinct adsorbed layers. The system with a single layer of CO_2 remains stable even at atmospheric pressures, indicating strong interactions between muscovite surfaces across the narrow gap created by the

Downloaded By: [University of California, Berkeley] At: 19:51 24 January 2011

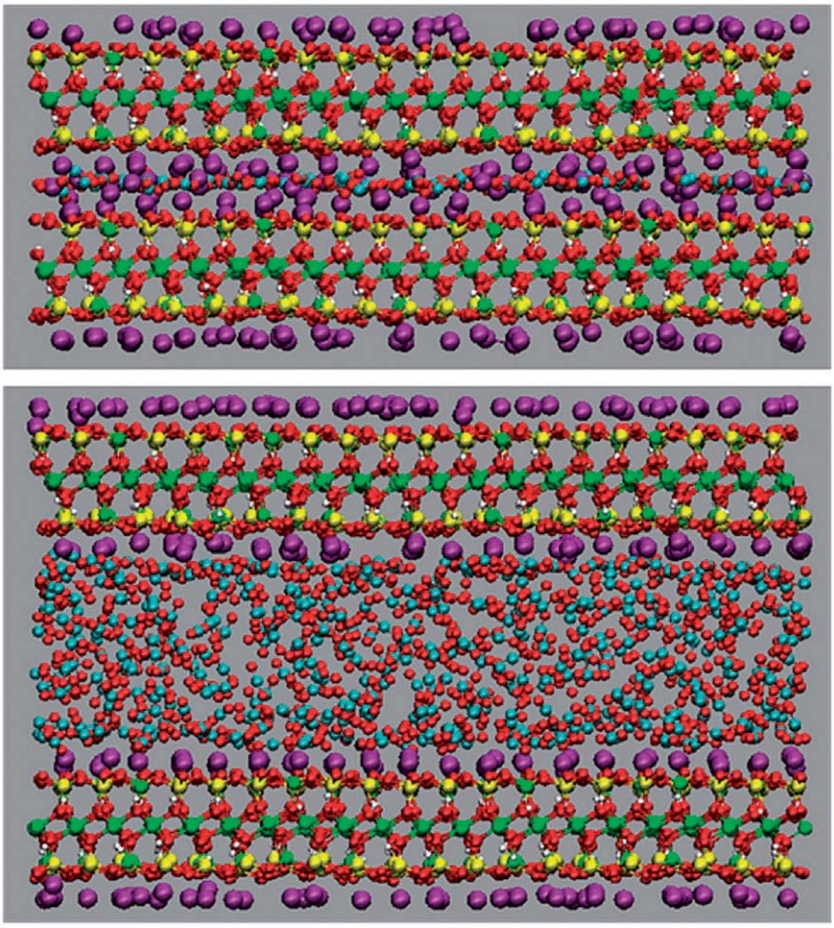

Figure 6. Carbon dioxide confined between muscovite plates. Top: single layer 2.467 g/cm^2 of CO_2. Bottom: 5×2.467 g/cm^2 of CO_2. C (cyan), O (red), K (purple), Si (yellow), Al (green) and H (white).

Downloaded By: [University of California, Berkeley] At: 19:51 24 January 2011

intercalated molecules. Larger quantities of CO_2 cause muscovite plates to separate at 1 bar. At gradually higher pressures, systems with increasing amounts of CO_2 lose their bulk characteristics and become compressed to a confined state with higher density. At 300 bars, in all systems studied up to 10×2.467 g/cm^2 the density of carbon dioxide in the interlayer reaches approximately 0.92 ± 0.02 g/cm^3. The only exception is the single-layered system, whose density is 1.01 g/cm^3 at all pressures. For comparison, the density of a bulk supercritical system at the same conditions is 0.83 g/cm^3 and the density of solid at -78.5°C is 1.56 g/cm^3. The expansion of the muscovite structure in the direction perpendicular to the pore surfaces upon absorbing a given amount of CO_2 is proportional to the pore width, H, listed in Table 3 minus the pore width with no CO_2 present (1.29 Å).

Figure 7 shows the density profiles of CO_2 atoms between parallel muscovite plates at various separations. It can be noticed that in the single-layered system the

Table 3. Self-diffusion coefficients of CO_2, D_{xy}, and pore widths, H, for systems with given amounts of CO_2 in slit pores as multiples of 2.467 g/cm^2. Format: D_{xy} [cm^2/s $\times 10^{-5}$]/H [Å].

$N \times 2.467$ g/cm^2	$P = 50$ bar	$P = 100$ bar	$P = 200$ bar	$P = 300$ bar
1	0.01/2.4	0.01/2.5	0.01/2.5	0.01/2.4
2	2.33/5.7	2.07/5.5	1.85/5.5	1.68/5.5
3	5.29/8.4	4.72/8.4	3.99/8.0	3.86/8.0
4	8.89/12.2	8.52/11.3	7.17/11.1	6.26/10.6
5	48.93/35.10	10.59/14.3	8.90/14.2	7.37/13.5
10	80.53/103.2	46.12/61.4	18.46/34.3	11.53/27.0

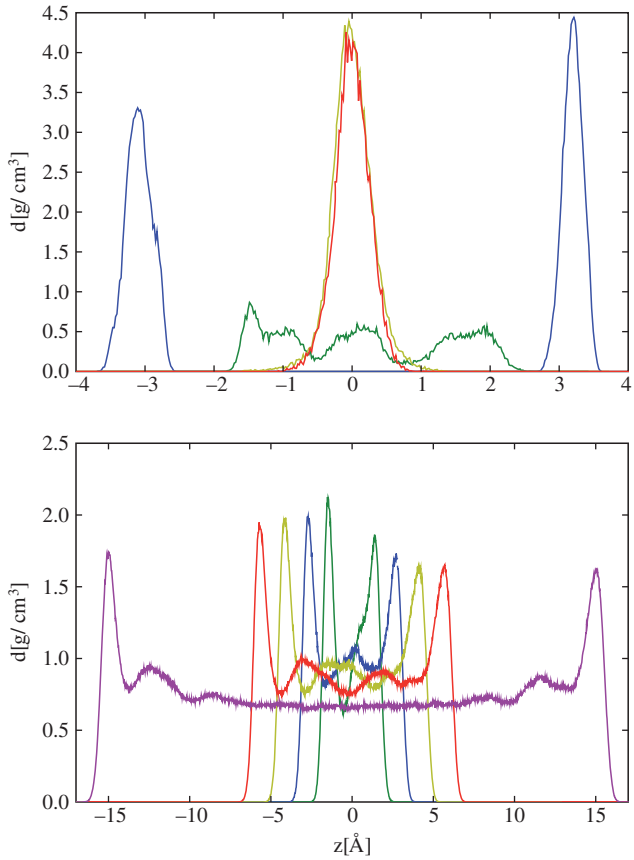

Figure 7. Density profiles of selected atoms between muscovite plates at $P = 200$ bar. Top: single layer of CO_2. Distributions of C (yellow), O (red), K (green), and Si (blue). Bottom: carbon distribution for N times 2.467 g/cm^2 CO_2, where N is 2 (green), 3 (blue), 4 (yellow), 5 (red), and 10 (magenta).

distribution of K^+ ions has three peaks. Ions occupying the center of the pore interact with both muscovite surfaces strongly enough to keep the crystal structure stable even with intercalated carbon dioxide. At pressures between 50 and 300 bars, increasingly greater amounts of confined CO_2 can form two, three, and four

Downloaded By: [University of California, Berkeley] At: 19:51 24 January 2011

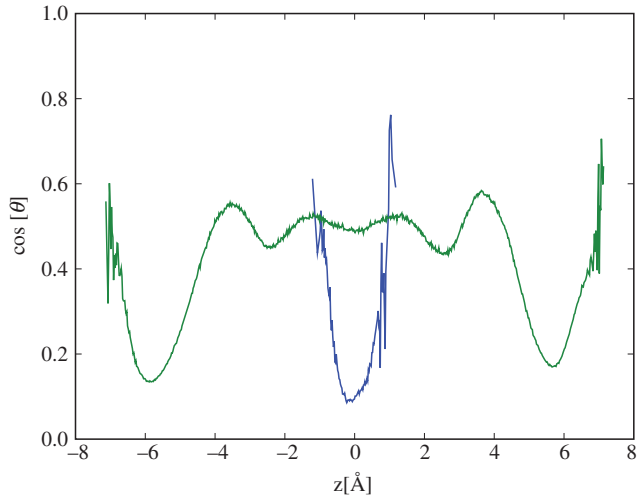

Figure 8. Orientation of CO_2 molecules expressed as the cosine of angle contained by the molecular axis and the normal to the surface plane at $T = 333$ K and $P = 200$ bar for 2.467 g/cm^2 CO_2 (blue), 5×2.467 g/cm^2 (green).

Downloaded By: [University of California, Berkeley] At: 19:51 24 January 2011

distinct ~3.0-Å thick layers with higher than bulk densities. At 200 bars (shown in Figure 7) the largest system forms a bulk-like region in the middle of the pore with approximately bulk densities (~0.68 g/cm^3) and three distinguishable layers at each surface.

The average orientation of CO_2 molecules in the slit pores is shown in Figure 8. The values of cos(Θ) close to 0 indicate that the molecular axis is oriented parallel to the surface, while values close to 1 correspond to the molecular axis orientation perpendicular to the surface. In the single-layered system, most CO_2 molecules lay flat between the muscovite plates. Similar behavior is also seen in the first layer of systems with wider pores. The oscillations of the orientational distribution reflect ordering of the supercritical fluid, which extends across more than 14 Å. Values of 0.6 and larger at close contact with the surfaces reveal the presence of molecules that are potentially capable of forming hydrogen bonds with hydroxyls buried under the surface layer.

An important question relates to chemical reactions of carbon dioxide with muscovite surfaces. As mentioned above, the initial step to the creation of surface carbonates is believed to be the interaction of CO_2 oxygens with protons of muscovite hydroxyls. We have seen indications of such hydrogen bonding in the orientational distribution (Figure 8). Inspection of the O–H pair distribution showed that the pair can approach as close as 1.8 Å but the interaction is very weak due to spatial constraints limiting the access of oxygens deeper below the muscovite surface. To test the effect of CO_2–muscovite cross parameters, we also performed simulations with LJ parameters rescaled to match those from [97] (see Table 2). In this case, the O–H distribution function forms a small but distinct peak at 1.8 Å, which is a clear sign of a hydrogen bond, albeit very weak. A more detailed study of bonding and subsequent reactions requires *ab initio* calculations or simulations with reactive forcefields, such as ReaxFF [100], which is beyond the scope of this contribution.

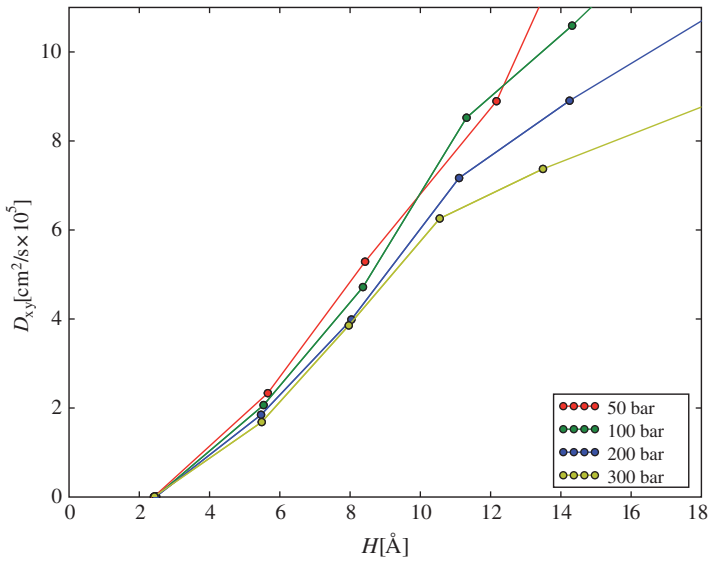

Figure 9. (Color online). Dependence of self-diffusion coefficient on the pore width for temperature 333 K at different pressures.

Additionally, when discussing realistic geologic systems, it is necessary to take into account water and other chemical paths leading to carbonates.

To assess the transport properties of supercritical carbon dioxide in muscovite slit pores, we calculated the self-diffusion coefficient parallel to the pore walls, D_{xy}, which can be obtained from the Einstein relation, $D_{xy} = \lim_{t\to\infty}\langle\Delta x^2(t) + \Delta y^2(t)\rangle/4t$, where Δx is the distance between particle positions at time 0 and t. The calculated values are listed in Table 3 along with pore widths (H). The relation between H, P, and D_{xy} is graphically represented in Figure 9. It shows that in narrow pores ($H < 12$ Å) and the investigated pressure range, the effect of pressure is relatively small, which can be attributed to small changes in average density. In wider pores with bulk-like regions in the center, pressure changes are also accompanied by larger density variations, which are reflected in diffusivity. For H below ~12 Å, the difference in D_{xy} between 50 and 300 bar is roughly 2×10^{-5} cm^2/s (25%). For H around 25 Å, D_{xy} nearly triples from 10×10^{-5} cm^2/s at 300 bar to 30×10^{-5} cm^2/s at 50. In the single-layered system ($H = 2.45$ Å), the diffusivity of CO_2 drops more than two orders of magnitude to $D_{xy} \sim 10^{-7}$ cm^2/s. As mentioned above, the layer is stable even at 1 bar and the diffusion rate remains the same (within the experimental error) as at higher pressures. CO_2 trapped in thin single-layer slit pores can be considered intercalated within muscovite crystal, whereas molecules in wider pores larger than 20 Å experience relatively free diffusion even at pressures expected in sequestration reservoirs.

5. Summary

Geological sequestration involves the capture, liquefaction, transport and injection of industrial CO_2 into deep geologic formation. The CO_2 may be injected into

Downloaded By: [University of California, Berkeley] At: 19:51 24 January 2011

brine aquifers, depleted oil or gas reservoirs and unmineable coal seam. Carbon dioxide is injected in a supercritical state that has much lower density and viscosity than indigenous fluids that it may displace. Regardless of the formation type, the CO_2 will encounter a complex heterogeneous porous matrix with widely varying pore size and pore distribution, interconnectivity, and surface composition. A small but non-trivial percentage of the pore space is comprised of voids that range from ~100 nm down to a few nm in size. These nanoporous environments are more dominant in the cap or seal rocks, such as shale or clay-rich mudstones, which act as confining barriers to leakage of CO_2 out of the storage reservoir. Although we have a very limited understanding of the nanoscale features found in most relevant subsurface lithologies particularly shale or clay-rich mudstones, progress has been made in delineating pore shape, size and distribution. Compositionally, shale can be categorized as a quartz-clay rock, simplifying to some extent the selection of nanoporous proxies used in experiments and simulations directed at emulating subsurface fluid–matrix interactions.

The size, distribution and connectivity of confined geometries, the chemistry of the solid (hydrophobicity versus hydophilicity), the chemistry of the fluids and their physical properties collectively dictate how CO_2 and other fluids migrate into and through these micro- and nano-environments, wet and ultimately react with the solid surfaces. The properties of simple and complex fluids confined in nanoporous earth materials can deviate significantly from bulk behavior under the same thermodynamic conditions. In this study, we focused our effort on the adsorption behavior of supercritical CO_2 in simple nanoporous materials (e.g. silica aerogel, muscovite) that act as proxies for more complex rock matrices. SANS results were described for sorption properties of supercritical CO_2 inside mesoporous silica aerogel. The Adsorbed Phase Model (APM) allows, for the first time, a means to quantify the physical properties (e.g. excess, absolute and total adsorption) of the adsorbed phase formed by fluids inside porous media in terms of the mean density and volume of the sorption phase. The results show clear evidence of fluid depletion for conditions above the critical density. By analogy to the well-established solvation behavior of a dilute near-critical solute, a theoretical framework was presented that describes the fundamental behavior of near-critical adsorption onto to a non-confining substrate. This assessment considered (a) an existing solvation formalism for highly compressible solvents (i.e. at near critical conditions) which provided a rigorous link between the strength of the solute–solvent interactions and the resulting solvent local density distribution and (b) that the confinement effects on the supercritical adsorption might be secondary due to the magnitude of the aerogel pore-size. Under these conditions, we were able to draw some simple yet useful connections between the observed experimental (NS) behavior and the predictions by integral equation calculations of Lennard–Jones fluids using the solvation analogy.

In practical terms, our results show that for a CO_2-only system, significant amounts can be sequestered at relatively low pressures and that the density of physisorbed CO_2 can be significantly higher (up to a factor of 3) than the bulk fluid.

Molecular dynamics simulations provide new insights into the structure and dynamics of supercritical CO_2 adsorbed into muscovite layers with varying width. At conditions expected in sequestration reservoirs (60°C, 200 bars), slit pores as wide as

Downloaded By: [University of California, Berkeley] At: 19:51 24 January 2011

15 Å are filled with higher-density CO_2 characterized by a layered structure and reduced diffusivity, whereas wider pores contain bulk-like highly mobile supercritical fluid. Space between cleaved muscovite surfaces separated by more than 5 Å provides a path for relatively free diffusion ($D > 10^{-5}\,cm^2/s$), but is unable to permanently capture molecular CO_2. To trap molecules in muscovite environment they must be either incorporated as a single layer in the crystal structure or, possibly, in thicker layers in the form of carbonate species created by a reaction with water. While we did not study free energy changes associated with intercalation to assess the thermodynamic aspect, existing industrial applications of supercritical CO_2 in montmorillonite suggest such processes are possible and can be expected in underground reservoirs.

Obviously, the substrates to be encountered during subsurface CO_2 injection will not consist of simple aerogel-type pores or muscovite slit pores, but by a more complex distribution of sizes, interconnectivities, and substrate chemistry. Therefore, the actual perturbations to fluid properties, such as adsorption, layering, H-bonding and diffusivity, result from the combination of many different partial structural and chemical contributions, i.e. some fluid properties will be profoundly impacted at certain length scales whereas others will not, depending on the extent of the confinement effects. By analyzing simple and well-characterized fluid–substrate systems, we are able to define some useful thermodynamic, structural and dynamic constraints while extracting meaningful microscopic information from theory and/or simulation to aid the subsequent nano- or mesoscopic modeling relevant to CO_2–matrix interactions.

Downloaded By: [University of California, Berkeley] At: 19:51 24 January 2011

Acknowledgements

Support for this work comes from the US Department of Energy through projects funded by the Office of Basic Energy Sciences: GRS (Section 3) from 'Structure and Dynamics of Earth Materials, Interfaces and Reactions' (FWP ERKCC72) and DRC (Section 1, 2, 3, 5), AAC (Section 4.1) and LV (Section 4.2) from ORNL's part of the LBNL 'Center for Nanoscale Control of Geologic CO_2' (FWP ERKCC67) under contract DE-AC05-00OR22725 to Oak Ridge National Laboratory, managed and operated by UT-Battelle, LLC. We thank two anonymous reviewers for their helpful comments and suggestions that improved this paper.

References

[1] S. Bachu, Environ.Geol. 44 (2003) p.277.
[2] R.P. Hepple and S.M. Benson, Environ. Geol. 47 (2005) p.576.
[3] S.M. Benson and D.R. Cole, Elements 4 (2008) p.325.
[4] S. M. Benson, M. Hoversten, E. Gasperikova and M. Haines, Proc. Int. Conf. Greenh. Gas Control Technol. (2005) p.640. Available at http://uregina.ca/ghgt7/PDF/papers/nonpeer/410.pdf
[5] R.M. Dilmore, R.M. Allen, D.E. McCarthy, J.R. Jones, S.W. Hedges and Y. Soong, Environ. Sci. Technol. 42 (2008) p.2760.
[6] Y. Leonenko and D.W. Keith, Environ. Sci. Technol. 42 (2008) p.2742.
[7] T.J. Katsube and M.A. Williamson, Clay Miner. 29 (1994) p.451.

[8] C.E. Neuzil, Water Resour. Res. 30 (1994) p.145.
[9] S.J. Sutton, F.G. Ethridge, W.R. Almon, W.C. Dawson and K.K. Edwards, AAPG Bull. 88 (2004) p.1185.
[10] O. Kwon, A.K. Kronenberg, A.F. Gangi, B. Johnson and B.E. Herbert, J. Geophys. Res. 109 (2004) p.B10205.
[11] Y. Yang and A.C. Aplin, J. Geophys. Res. 112 (2007) p.B03206.
[12] J.M. Ketzer, B. Carpentier, Y. Le Gallo and P. Le Thiez, Oil Gas Sci. Technol. Rev. IFP 60 (2005) p.259.
[13] A. Hildenbrand, S. Schlömer, B.M. Krooss and R. Littke, Geofluids 4 (2004) p.61.
[14] A. Busch, S. Alles, Y. Gensterblum, D. Prinz, D.N. Dewhurst, M.D. Raven, H. Stanjek and B.M. Kroos, Int. J. Greenh. Gas Control Technol. 2 (2008) p.297.
[15] G. Sposito, S.H. Park and R. Sutton, Clays Clay Miner. 47 (1999) p.192.
[16] J. Wang, A. Kalinichev and R. Kirkpatrick, Earth Plan. Sci. Lett. 222 (2004) p.517.
[17] J. Wang, A. Kalinichev and R. Kirkpatrick, Geochim. Cosmochim. Acta 68 (2004) p.3351.
[18] J. Wang, A. Kalinichev, R. Kirkpatrick and R. Cygan, J. Phys. Chem. B 109 (2005) p.15893.
[19] J. Wang, A. Kalinichev and R. Kirkpatrick, Geochim. Cosmoschim. Acta 70 (2006) p.562.
[20] D. Dysthe and R. Wogelius, Chem. Geol. 230 (2006) p.175.
[21] D.R. Cole, K. Herwig, E. Mamontov and J. Larese, *Neutron scattering and diffraction studies of fluids and fluid-solid interactions*, in *Neutrons Scattering in Earth Sciences*, Vol. 63, Reviews in Mineralogy and Geochemistry, H.-R. Wenk, ed., Washington, DC, 2006, p.313.
[22] N. Malikova, A. Cadene, E. Dubois, V. Marry, S. Durand-Vidal, P. Turq, J. Breu, S. Longville and J.-M. Zanotti, J. Phys. Chem. C 111 (2007) p.17603.
[23] D.R. Cole, E. Mamontov and G. Rother, *Structure and dynamics of fluids in microporous earth and engineered materials*, in *Neutron Applications in Earth, Energy and Environmental Sciences*, L. Liang, R. Rinaldi and H. Schober, eds., Springer, Berlin, 2009, p.547.
[24] J.W. Johnson, J.J. Nitao and J.P. Morris, *Reactive transport modeling of cap-rock integrity during natural and engineered CO_2 storage*, in *Carbon Dioxide Capture for Storage in Deep Geologic Formations*, Vol. 2, D.C. Thomas and S.M. Benson, eds., Elsevier, Amsterdam, 2005, p.787.
[25] W. Dawson and W.R. Almon, GCAGS Trans. 52 (2002) p.167.
[26] A.C. Aplin, I.F. Matenaar, D.K. McCarty and B.A. van der Pluum, Clays Clay Miner. 54 (2006) p.500.
[27] N.H. Mondol, K. Bjorlykke, J. Jahren and K. Hoeg, Mar. Petrol. Geol. 24 (2007) p.289.
[28] P. de Caritat, J. Bloch, I. Hutcheon, F.J. Longstaffe and H.J. Abercrombie, Clays Clay Miner. 45 (1997) p.327.
[29] R.A. Chadwick, P. Zweigel, U. Gregersen, G.A. Kirby, S. Holloway and P.N. Johannssen, Energy 29 (2004) p.1371.
[30] S. Boggs Jr, *Petrology of Sedimentary Rocks*, Cambridge University Press, Cambridge, UK, 2009.
[31] Y. Yang and A.C. Aplin, Petrol. Geosci. 10 (2004) p.153.
[32] D.J.K. Ross and R.M. Bustin, Mar. Petrol. Geol. 26 (2009) p.916.
[33] A. Busch, S. Alles, B.M. Kroos, H. Stanjek and D. Dewhurst, Energy Procedia 1 (2009) p.3229.
[34] T. Fujii, Y. Satot, H. Lin, K. Sasaki, T. Takahashi, H. Inomata and T. Hashida, CP898, Water Dynamics: 4th International Workshop on Water Dynamics, 2007, p.79.
[35] A. Busch, Y. Gensterblum and B.M. Krooss, Energy Fuels 21 (2007) p.1640.
[36] E. Ozdemir and K. Schroeder, Energy Fuels 23 (2009) p.2821.

Downloaded By: [University of California, Berkeley] At: 19:51 24 January 2011

[37] Y.B. Melnichenko, A.P. Radlinski, M. Mastalerz, G. Cheng and J. Rupp, Int. J. Coal Geol. 77 (2009) p.69.
[38] M.S. Gruszkiewicz, M.T. Naney, J.G. Blencoe, D.R. Cole, J.C. Pashin and R.E. Carroll, Int. J. Coal Geol. 77 (2009) p.23.
[39] K. Jessen, G.-Q. Tang and A.R. Kovscek, Transp. Porous Med. 73 (2008) p.141.
[40] K.S.W. Sing, D.H. Everett, R.A.W. Haul, L. Moscou, R.A. Pierotti, J. Rouquerol and T. Siemieniewska, Pure Appl. Chem. 57 (1985) p.603.
[41] M.D. Donohue and G.L. Aranovich, Adv. Colloid. Interface Sci. 76/77 (1998) p.137.
[42] L. Zhou, Y. Zhou, S. Bai and B. Yang, J. Colloid. Interface Sci. 253 (2002) p.9.
[43] L. Zhou, Y. Zhou, S. Bai and B. Yang, Adsorption 8 (2002) p.125.
[44] L. Zhou, S. Bai and W. Su, Langmuir 19 (2003) p.2683.
[45] O. Di Giovanni, W. Dörfler, M. Mazzotti and M. Morbidelli, Langmuir 17 (2001) p.4316.
[46] N. Tatsuda, Y. Goto, N. Setoyama and Y. Fukushima, Adsorp. Sci. Technol. 23 (2005) p.763.
[47] R. Pini, S. Ottiger, A. Rajendran, G. Storti and M. Mazzotti, Adsorption 14 (2008) p.133.
[48] P. van Hemert, H. Bruining, E.S.J. Rudolph, K.-H.A.A. Wolf and J.G. Maas, Rev. Sci. Instrum. 80 (2009) p.035103.
[49] Ch. Chilev, B. Weinberger, J.Ph. Passarello, F.D. Darkrim Lamari and I. Pentchev, AIChe J. 55 (2009) p.1793.
[50] S. Liu and X. Yang, J. Chem. Phys. 124 (2006) p.244705.
[51] F.N. Ridha and P.A. Webley, Separ. Purif. Technol. 67 (2009) p.336.
[52] J.H. Chen, D.S.H. Wong, C.S. Tan, R. Subramanian, C.T. Lira and M. Orth, Ind. Eng. Chem. Res. 36 (1997) p.2808.
[53] R. Humayun and D.L. Tomasko, Thermodynamics 46 (2000) p.2065.
[54] M. Thommes, G.H. Findenegg and H. Lewandowski, Ber. Bunsen-Ges. Phys. Chem. 98 (1994) p.477.
[55] M. Thommes, G.H. Findenegg and M. Schoen, Langmuir 11 (1995) p.2137.
[56] W.D. Machin, Langmuir 15 (1999) p.169.
[57] C.R. Yonker and R.D. Smith, J. Chromatogr. 550 (1991) p.775.
[58] O. Sel, A. Brandt, D. Wallacher, M. Thommes and B. Smarsly, Langmuir 23 (2007) p.4724.
[59] Y.B. Melnichenko, G.D. Wignall, D.R. Cole and H. Frielinghaus, J. Chem. Phys. 124 (2006) p.204711.
[60] G. Rother, Y.B. Melnichenko, D.R. Cole, H. Frielinghaus and G.D. Wignall, J. Phys. Chem. C 111 (2007) p.15736.
[61] W.-L. Wu, Polymer 23 (1982) p.1907.
[62] M.S. Schneider, J.-D. Grunwaldt and A. Baiker, Langmuir 20 (2004) p.2890.
[63] D.D. Do, H.D. Do and D. Nicholson, J. Phys. Chem. B 113 (2009) p.1030.
[64] B. Coasne and R.J.M. Pellenq, J. Chem. Phys. 120 (2004) p.2913.
[65] X.N. Yang and X.P. Yue, Colloid Surf. A 301 (2007) p.166.
[66] A. Vishnyakov, Y.Y. Shen and M.S. Tomassone, J. Chem. Phys. 129 (2008) p.174704.
[67] A. Brodka and T.W. Zerda, J. Chem. Phys. 95 (1991) p.3710.
[68] X.N. Yang, Z.J. Xu and C.J. Zhang, J. Colloid. Interface Sci. 297 (2006) p.38.
[69] J. Puibasset and R.J.M. Pellenq, Phys. Chem. Chem. Phys. 6 (2004) p.1933.
[70] N. Giovambattista, P.G. Debenedetti and P.J. Rossky, J. Phys. Chem. C 111 (2007) p.1323.
[71] N. Giovambattista, P.J. Rossky and P.G. Debenedetti, Phys. Rev. Lett. 102 (2009) p.050603.

Downloaded By: [University of California, Berkeley] At: 19:51 24 January 2011

[72] A. Goj, D.S. Sholl, E.D. Akten and D. Kohen, J. Phys. Chem. B 106 (2002) p.8367.
[73] D.A. Litton and S.H. Garofalini, J. Appl. Phys. 89 (2001) p.6013.
[74] Y. Qin, X.N. Yang, Y.F. Zhu and J.L. Ping, J. Phys. Chem. C 112 (2008) p.12815.
[75] V.A. Bakaev and W.A. Steele, J. Chem. Phys. 111 (1999) p.9803.
[76] E.A. Leed and C.G. Pantano, J. Non-Cryst. Solids 325 (2003) p.48.
[77] V.A. Bakaev, W.A. Steele, T.I. Bakaeva and C.G. Pantano, J. Chem. Phys. 111 (1999) p.9813.
[78] A. Oleinikova and I. Brovchenko, Phys. Rev. E 78 (2008) p.061601.
[79] A.A. Chialvo and P.T. Cummings, AIChe J. 40 (1994) p.1558.
[80] D. Nicholson and N.G. Parsonage, *Computer Simulation and Statistical Mechanics of Adsorption*, Academic Press, New York, 1982.
[81] J.G. Kirkwood and F.P. Buff, J. Chem. Phys. 19 (1951) p.774.
[82] P.G. Debenedetti and R.S. Mohamed, J. Chem. Phys. 90 (1989) p.4528.
[83] P.G. Debenedetti and A.A. Chialvo, J. Chem. Phys. 97 (1992) p.504.
[84] A.A. Chialvo, J. Phys. Chem. 97 (1993) p.2740.
[85] A.A. Chialvo and P.T. Cummings, Mol. Phys. 84 (1995) p.41.
[86] D.B. McGuigan and P.A. Monson, Fluid Phase Equilibr. 57 (1990) p.227.
[87] I.B. Petsche and P.G. Debenedetti, J. Phys. Chem. 95 (1991) p.386.
[88] H. Poppa and A.G. Elliot, Surf. Sci. 24 (1971) p.149.
[89] K.G. Bhattacharyya, Langmuir 5 (1989) p.1155.
[90] H.K. Christenson, J. Phys. Chem. 97 (1993) p.12034.
[91] F. Ostendorf, C. Schmitz, S. Hirth, A. Kuhnle, J.J. Kolodziej and M. Reichling, Nanotechnology 19 (2008) p.305705.
[92] G.K. Serhatkulu, C. Dilek and E. Gulari, J. Supercrit. Fluids 39 (2006) p.264.
[93] M. Zhang, L. Wang, S. Hirai, S.A.T. Redfern and E.K.H. Salje, Am. Miner. 90 (2005) p.173.
[94] X. Peng, J. Zhao and D. Cao, J. Colloid. Interface Sci. 310 (2007) p.391.
[95] X. Yang and C. Zhang, Chem. Phys. Lett. 407 (2005) p.427.
[96] J.G. Harris and K.H. Yung, J. Phys. Chem. 99 (1995) p.12021.
[97] Y. Qin, X. Yang, Y. Zhu and J. Ping, J. Phys. Chem. C 112 (2008) p.12815.
[98] H. Heinz, H. Koerner, K.L. Anderson, R.A. Vaia and B.L. Farmer, Chem. Mater. 17 (2005) p.5658.
[99] S.J. Plimpton, J. Comp. Phys. 117 (1995) p.1.
[100] A.C.T. van Duin, A. Strachan, S. Stewman, Q.S. Zhang, X. Xu and W.A. Goddard, J. Phys. Chem. A 107 (2003) p.3807.
[101] D.A. McQuarrie, *Statistical Mechanics*, Harper and Row, New York, 1976.
[102] R. Rothbauer, Neues. Jahrb. Miner. Monatsh. (1971) p.143.
[103] R. Lynch, Clays Clay Miner. 45 (1997) p.618.
[104] O. Kwon, A.K. Kronenberg, A.F. Gangi and B. Johnson, J. Geophys. Res. 106 (2001) p.19339.
[105] M.L.W. Tuttle and G.N. Breit, App. Geochem. 24 (2009) p.1549.
[106] R.A. Xhadwick, P. Zweigel, U. Gregersen, G.A. Kirby, S. Holloway and P.N. Johannessen, Energy 29 (2004) p.1371.
[107] M. Anegeli, M. Soldal, E. Skurtveit and E. Aker, Energy Procedia 1 (2009) p.3351.
[108] D.N. Dewhurst, R.M. Jones and M.D. Raven, Petrol. Geosci. (2002) p.371.
[109] R. Nygård, M. Gutierrez, K. Høeg and K. Bjørlykke, Petrol. Geosci. 10 (2004) p.259.
[110] F. Cavalcante, S. Fiore, G. Piccarreta and F. Tateo, Clay Min. 38 (2003) p.383.

Downloaded By: [University of California, Berkeley] At: 19:51 24 January 2011

Appendix 1. Relevant theoretical results linking substrate adsorption with the solvation analogy

Our main goal is to make contact between the density dependence of the excess function $n_e(\rho_b)$, i.e.

$$n_e(\rho_b) = \int_0^l (\rho(z) - \rho_b)\mathrm{d}V \tag{3}$$

and the conventional Kirkwood–Buff integral G_{sf}^{∞}, where the upper limit is usually $l \to \infty$ in the general case, but obviously finite under the box-model framework [27]. A simple reorganization of Equation (3) yields

$$n_e(\rho_b) = \rho_b \int_0^l (g(z) - 1)\mathrm{d}V, \tag{4}$$

where $g(z) \equiv \rho(z)/\rho_b$ is the axial distribution function of the solvent at a distance z from the surface. Note that, under the above-suggested definition, (4) is equivalent to $\Gamma = \rho_b G_{sf}^{\infty}$ in the Kirkwood–Buff based solvation formalism [85]. Moreover, its density dependence follows immediately from the expansion [101]:

$$\begin{aligned} g(z) &= \exp(-u(z)/kT)\exp(-\Delta\omega(z)/kT) \\ &\cong \exp(-u(z)/kT)(1 + a\rho_\rho + b\rho_\rho^2 + \cdots h.o.t). \end{aligned} \tag{5}$$

Consequently,

$$n_e(\rho_b \to 0) = \rho_b \int_0^{\infty} (\exp(-u(z)/kT) - 1)\mathrm{d}V = -2\rho_b B_{sf}(T) > 0, \tag{6}$$

where $B_{sf}(T)$ is the corresponding second virial coefficient. Moreover, the corresponding slopes become

$$(\partial n_e/\partial \rho_b)_{\rho_b \to 0} = \int_0^{\infty} (\exp(-u(z)/kT) - 1)\mathrm{d}V = -2B_{sf}(T) > 0. \tag{7}$$

Similarly, Equation (7) can be recast by invoking a loose definition of the Henry constant [17], i.e.

$$(\partial n_e/\partial P)_{P \to 0} = -2B_{sf}(T)/kT \equiv H(T). \tag{8}$$

Downloaded By: [University of California, Berkeley] At: 19:51 24 January 2011